Droplet Injection, Heating, and Combustion

Shaik Sajeed Hussain *, Phani Raghava Panchagnula †, and Gaojun Yu ‡
Institut Supérieur de l'Aéronautique et de l'Espace, Toulouse, France, 31400

I. Droplet Transport by Unsteady, Turbulent Flow

Using `Ansys Fluent`, 2D, axisymmetric, turbulent droplet injections is simulated. The air enters the domain at $u_0 = 0.32\frac{m}{s}$, $T_g = 250K$ and $p = p_{atm} = 101325Pa = 1bar$. Five particles are injected into the domain at $u_{p,x} = 7.5\frac{m}{s}$ and $u_{p,y} = 3.8\frac{m}{s}$, where $u_{p,x}$ and $u_{p,y}$ are the stream-wise and transversal component of particle velocities. The droplets are of diameters: 1, 10, 50, 100 and 150 μm. The boundary conditions used are shown in Fig. 1. The turbulence model used is $k-\omega$ SST model.

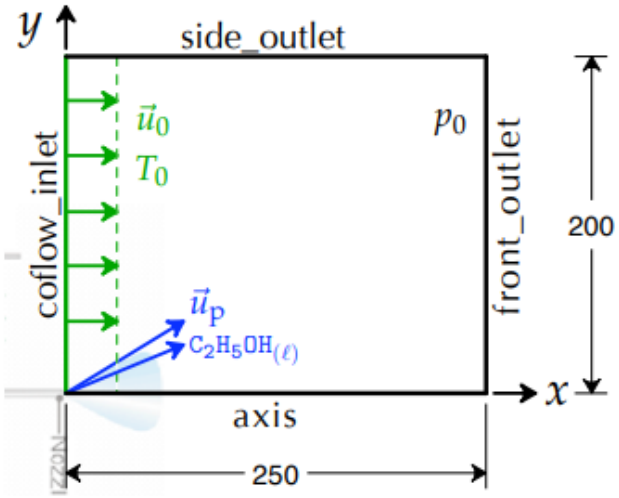

Fig. 1 Burner configuration and BC set up.

Injection position, velocity, particle diameter, temperature, and particle mass for each particle are defined in a text file which is imported into the `Ansys Fluent`. The injection file has the following syntax, each line representing one particle

```
1      ( ( x y z ux uy uz dp Tp Mass ) name )
```

The boundary conditions must also be set for the droplets with a *discrete phase model* (DPM) approach. An *escape* BC has been used at both the domain outlets, which means the particles exit the domain interacting with the wall or bounce back. It is necessary to calculate the flow properties at each point of the computational grid to retrieve each particle position by the solver. Flow is steady, so the properties are constant and homogeneous across the domain, so it is not mandatory to run the flow solver. In a case of unsteady solver, to calculate the trajectories of the particles, `Fluent` runs the DPM together with the flow solver, as, indeed, the trajectories are strong function of the flow properties. This approach is called *one-way coupling*. In case of a steady solver `Fluent` does not even need to run the `RANS` solver, as the gas properties are everywhere constant and equal to the initial conditions.

*MSc Student, Département Aérodynamique, Énergétique et Propulsion
†MSc Student, Département Aérodynamique, Énergétique et Propulsion
‡MSc Student, Département Aérodynamique, Énergétique et Propulsion

A. Relaxation Time

The particle transport equation is:

$$\frac{d\mathbf{u}}{dt} = \frac{1}{\tau_p}(\mathbf{u_g}(\mathbf{x_p}, \mathbf{t}) - \mathbf{u_p}) \tag{1}$$

where $\tau_p = \frac{1}{C_D}\frac{24}{Re_p}\frac{\rho_l d_p^2}{18\mu_g}$ is the particle's relaxation time and $Re_p = \frac{\rho_g d_p}{\mu_g}|\mathbf{u_g} - \mathbf{u_p}|$ is Reynolds number. Under the condtion of $Re_p \ll 1$ [1], the drag coefficient C_d can be written out as:

$$C_D = \frac{24}{Re_p} \tag{2}$$

also called *Stokes Law*. Using the Stokes Law and expression of τ_p:

$$\tau_p = \frac{\rho_l d_p^2}{18\mu_g} \tag{3}$$

The results are given in Tab. 1.

Table 1 Relaxation time as a function of particle diameter (d_p), calculated with Eq. 3 and graphical estimation.

$\boldsymbol{d_p}\,(\mu m)$	$\boldsymbol{\tau_p}\,(s)$	$\boldsymbol{\tau_p}\,(s)$, Graphic
1	2.551×10^{-6}	3.2×10^{-6}
10	2.551×10^{-4}	1.8×10^{-4}
50	6.379×10^{-3}	2.85×10^{-3}
100	2.551×10^{-2}	9.14×10^{-2}
150	5.741×10^{-2}	1.6×10^{-2}

The relaxation time represents the time for the particles' velocity to drop consistently due to flow drag. Even though Eq. (3) is derived from Stokes law, the graphical estimation does not agree with the analytical estimation. This is because the assumption of the Reynolds Number is not really respected when particle diameter is increased. The graphical results are tabulated in 1. At small diameters the results do not differ, as the Reynolds Number is small and the Stokes Law is still fairly valid.

B. Turbulent Dispersion

The equations being resolved are `RANS`, therefore each field f is divided into a time-averaged component $\bar{f}$ and instantaneous fluctuations component f', out of which only the time-averaged component is solved and the fluctuation part is modeled through the turbulence model. In this case, to retrieve the instantaneous velocity at each particle position x_p for a given value of k and ω, it is necessary to introduce a *turbulent dispersion model* ("Eddy Life Time"). Albeit the turbulence model has been activated, the droplets' trajectories without the turbulent dispersion model suggest that the flow might be laminar, which is not true in real. The solver only takes into account the time-averaged variables and requires an additional model to take turbulence into account throughout the droplet transport.

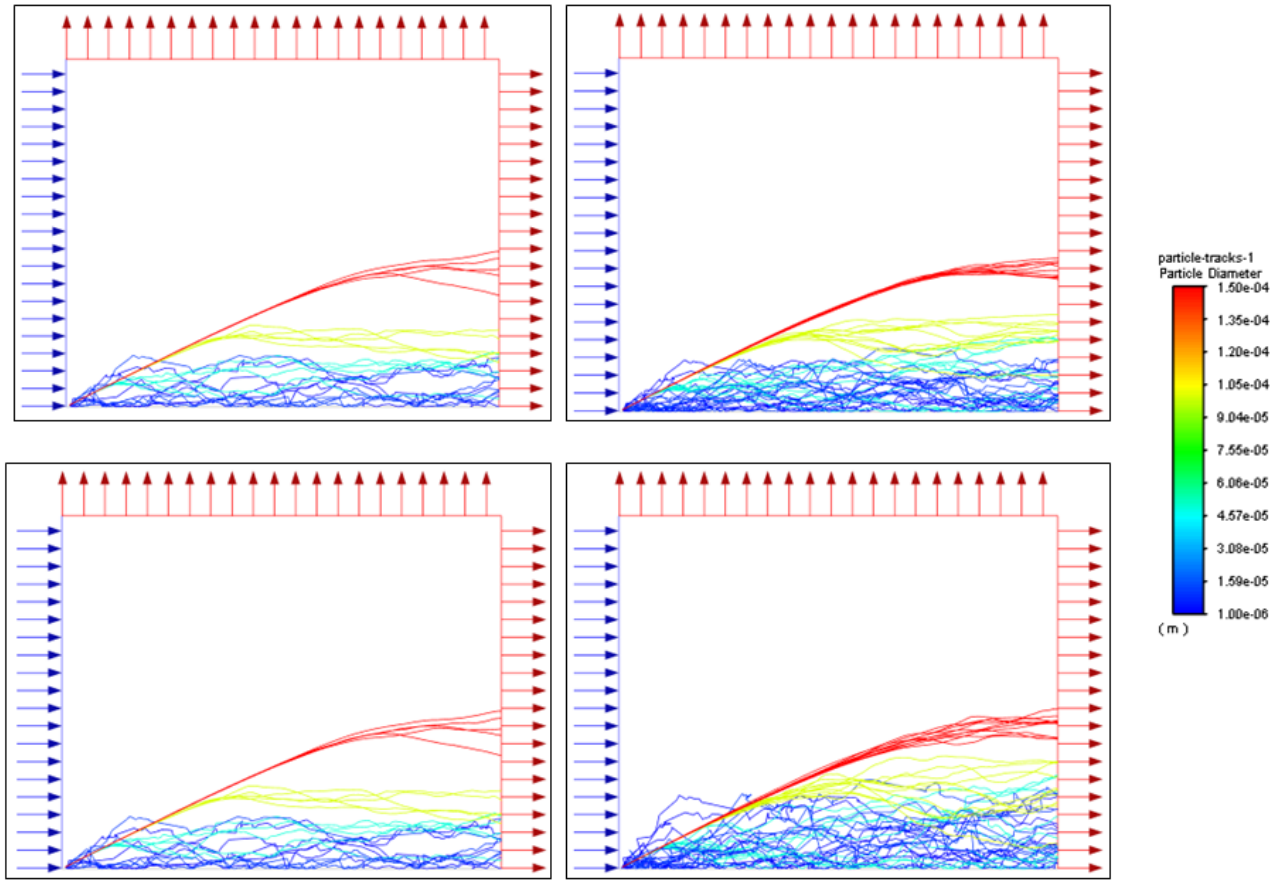

Fig. 2 Particle Tracks - trajectory for different values of "Number of Tries" (in the turbulent dispersion model 5 tries on the left and 10 tries on the right) and Turbulent Kinetic Energy (TKE). On the top, $k = 0.05\frac{m^2}{s^2}$, whereas, on the bottom, $k = 0.1\frac{m^2}{s^2}$.

When the turbulent dispersion model is activated, the particles continue to drift rightward along with the gas flow. However, the addition of random fluctuations to the gas's velocity introduces movement in various directions, leading to a broader spread of the stream. This broadening aligns more closely with real-world behavior. For instance, the effect of the initial total turbulent kinetic energy on particle trajectories is illustrated in Figure 2. Simply put, a higher initial TKE levels the distribution of velocity fluctuations, thereby increasing the likelihood of encountering a broader spectrum of velocities.

C. Droplet Transport by an Unsteady Flow

This section focuses on the unsteady behavior of the flow after the injection in a configuration as the one illustrated in Fig 3. The inlet mass flow rate of 4.75 $\frac{Kg}{s}$ at $T = 1160K$, which subsequently evacuates the domain at $p = 3.15bar$. The instability within the duct stems from the initiation of separation at the flame holder's side branches, which results in turbulent flow and recirculation in the area downstream. At location I (referenced in Fig. 3), five kerosene droplets of varying diameters—1, 3, 10, 20, and 50—are introduced. Consistent with the previous section, the turbulence is modeled using the $k - \omega$ SST approach.

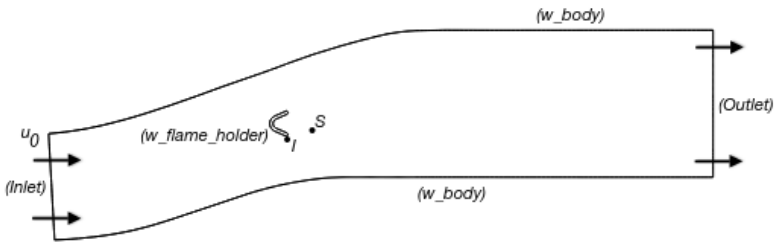

Fig. 3 Computational domain for a V-shaped flame holder in an annular duct.

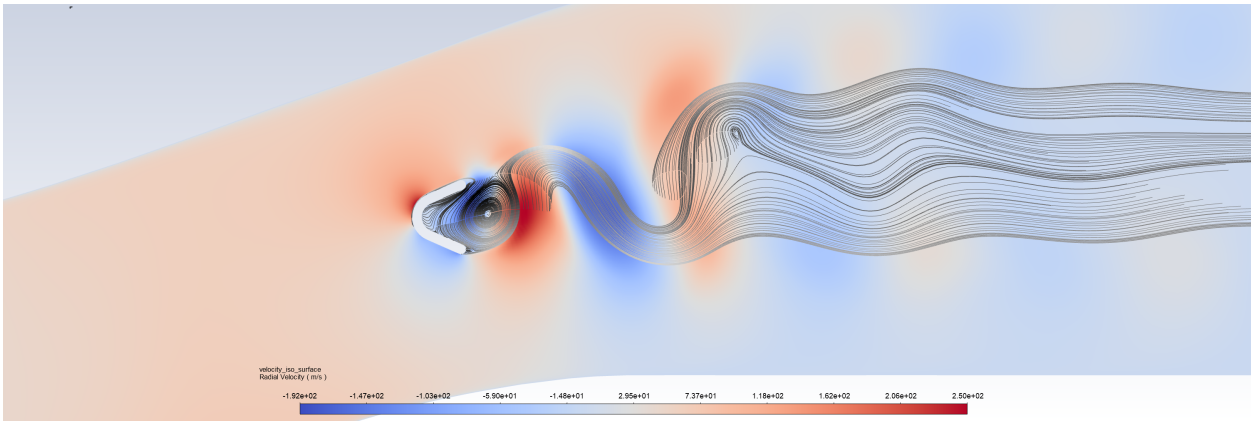

Fig. 4 An instantaneous recirculation bubble is depicted alongside the contour of the instantaneous transverse velocity.

Figure 4 captures a momentary view of the flow pattern downstream from the flame holder, where the flow undergoes separation at the tips and exhibits periodic interactions within the valley-shaped core, leading to the formation of a wake downstream.

D. Droplet Trajectories in the unsteady flow

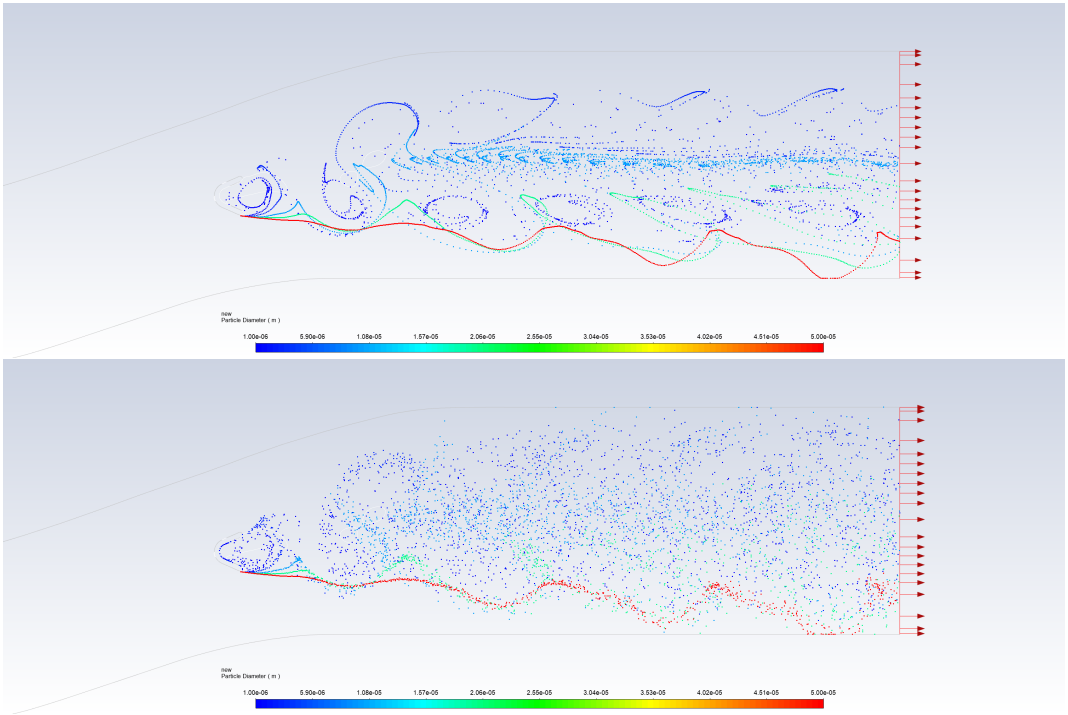

Fig. 5 Particle trajectories colored by the particle diameter, both with and without dispersion.

As depicted in Fig. 5, the simulation's solver presents only the final state at $t = 5ms$, focusing specifically on the pathlines. For example, the red particles, which are the heaviest, do not simply follow the downstream flow due to their significant mass and inertia, which tend to maintain their initial paths. Furthermore, they experience less drag, in line with Stokes' Law (referenced in Eq. 2). On the other hand, the blue trajectories represent lighter particles that are less able to resist the prevailing flow and thus are carried along with the streamlines.

E. Stokes Number

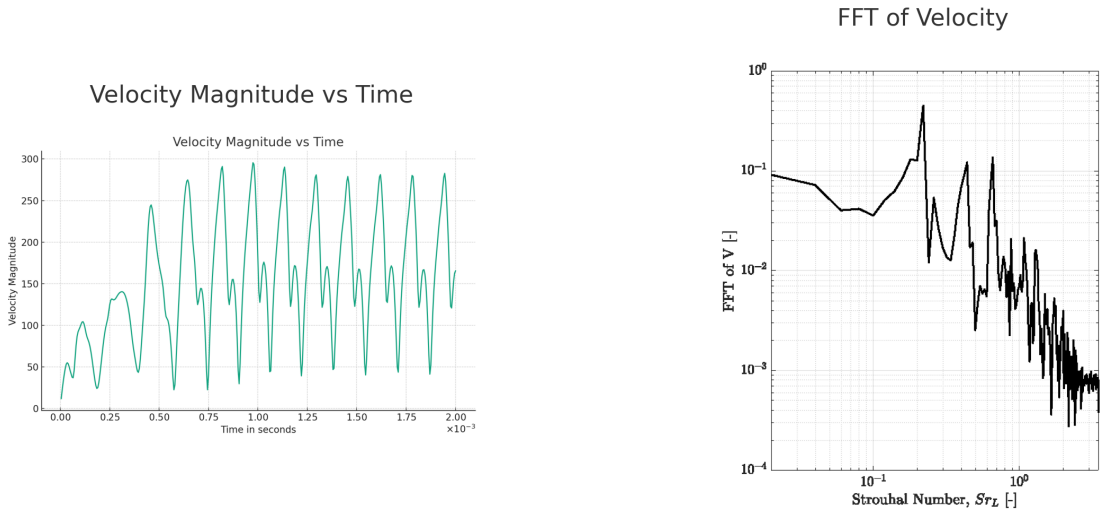

Fig. 6 (Left) Velocity magnitude at point S (see Fig. 3) and (right) the corresponding FFT.

From Fig 6, the dominant frequency, expressed as non-dimensional Strouhal Number, of $St \sim 0.21$, very similar to the typical vortex shedding Strouhal Number, amounting to 0.2. From the dominant frequency, it is possible to calculate the period of oscillation as:

$$\tau_g = \frac{1}{f_g} = 1.5954 \times 10^{-4} s \tag{4}$$

Assuming $\rho_l = 780 \frac{Kg}{m^3}$ $\mu = 4.6 \times 10^{-5}$ and using the Stokes Law, we can calculate the relaxation times for the particles by using Eq. 3. Let us define the Stokes Number as:

$$St = \frac{\tau_p}{\tau_g} \tag{5}$$

The results of both calculations are summarised in Tab. 2. The Stokes number is function of diameter. When the Stokes Number is less than one, the particle undergoes pure advection, without being able to counteract, thus following the flow streamlines and when the Stokes number is greater than one, the particle's inertia is enough to follow its proper trajectory. In summary, a particle characterized by a low Stokes number will follow the streamlines (complete advection), whereas a particle with a high Stokes number will be primarily influenced by its own inertia and maintain its original path. Additionally, it's important to note that the Stokes Number can be related to various time scales, hence it is crucial to clarify the particular time scale being referred to when defining it.

Table 2 Particle relaxation times and corresponding Stokes Number based on the flow time scale presented in Eq. 4.

$d_p(\mu m)$	$\tau_p(s)$	$St(--)$
1	9.4202×10^{-7}	0.0059
10	8.4782×10^{-6}	0.0531
50	9.4202×10^{-5}	0.5905
100	3.7681×10^{-4}	2.3619
150	2.3550×10^{-3}	14.7616

F. Another Stokes Number

The Stokes Number can be defined with different time scales.

The turbulent time scale τ_ω is:

$$\tau_\omega = \sqrt{\frac{3}{2}} C_\mu^{-\frac{1}{4}} \frac{1}{\omega} \tag{6}$$

where $C_\mu^{-\frac{1}{4}} = 0.09$ and $\omega = 10^{-5} s^{-1}$ is the dissipation rate at the point S in the unsteady simulation.

Table 3 Particle relaxation times and corresponding Stokes Number based on the turbulent time scale presented in Eq. 6.

$d_p\,(\mu m)$	$\tau_p\,(s)$	$St(--)$
1	9.4202×10^{-7}	0.0421
10	8.4782×10^{-6}	0.3792
50	9.4202×10^{-5}	4.2129
100	3.7681×10^{-4}	16.8515
150	2.3550×10^{-3}	105.3220

Primarily, the turbulent Stokes Number is an order of magnitude higher than the Stokes Number based on flow. Consequently, as anticipated, turbulence intensifies the particle's inertial effects, leading to increased disorder within the flow. Due to turbulence, it becomes less probable for the droplets to track the fluid streamlines closely. It's also worth noting that in scenarios such as PIV (Particle Image Velocimetry) measurements, the Stokes Number is indicative of the level of fidelity with which particles can trace the flow. To achieve accurate tracing, the particle's response time must be quicker than the flow's smallest time scale. Lower Stokes numbers correlate with enhanced tracing precision; with $St >> 1$, particles tend to separate from the flow, particularly in areas of rapid deceleration. Conversely, with $St << 1$, particles adhere closely to the flow streamlines.

II. Practical 4: Droplet Heating and Evaporation

A. Introduction

In accordance with the previous work outlined in Figure 1, we use same configuration wherein air is introduced into the system with a velocity of 32 m/s, alongside a gas temperature (T_g) of 500 K and a gas pressure (p_g) of 101,325 Pa. The flow regime under consideration adheres to laminar, 2D with axi-symmetric properties. We examine the behavior of ethanol droplets injected into the airflow from the lower left corner. The droplets are specified to possess a uniform temperature (T_p) of 250 K upon injection, with initial velocity components of $u_{p,x} = 7.5$ m/s and $u_{p,y} = 3.8$ m/s, directed horizontally and vertically, respectively. Droplet sizes are diversified across five distinct categories, ranging from 1 μm to 150 μm in diameter. These variations serve to provide comprehensive insights into the impact of droplet size on subsequent flow dynamics and interaction with the surrounding air medium with the Y_{O2}, is set to 0.23 at initialization.

B. Understanding droplet heating and evaporation models in Fluent

Fluent utilizes two critical temperature thresholds: the vaporization temperature (T_{vap}) and the boiling temperature (T_{b}). These thresholds determine how droplets behave based on their temperature.

- When the particle temperature (T_{p}) is below T_{vap} (law 1), the droplet does not evaporate but can experience heating.
- If $T_{\text{vap}} < T_{\text{p}} < T_{\text{b}}$ (law 2), the droplet follows an infinite conduction model for evaporation which considers an infinite value for the thermal conduction inside the droplet. As a consequence, the droplet temperature is uniform, but time varying and conservation of energy inside the droplet gives:

$$Q_l = \frac{\pi D_d^3}{6} \rho_l C_{pl} \frac{dT_l}{dt} \tag{7}$$

If the heating of the droplet is significant, the surface temperature might be underestimated because all the energy is immediately conducted to the entire droplet. This situation also affects the estimation of the vaporization mass flow rate.

- When $T_p \geq T_b$ (law 3), the particle temperature stabilizes at the liquid's boiling temperature, and the evaporation rate follows a d^2 law with a constant K_d, incorporating the Ranz and Marshall correlation for convective heat transfer. The d^2 law of evaporation rate, with $d_{p,0}^2$ as the initial particle diameter, is expressed as:

$$d_p^2 = d_{p,0}^2 - K_d \cdot t \tag{8}$$

C. One-way-coupling droplet heating and evaporation

With assumption for the flow being steady and homogeneous, only DPM model can be used by plotting particle tracks instead of running the flow solver. In order to determine the particle heating time scale, the abscissa of the 63% of the maximum temperature provides the time scale. It's important to note that the percentage is taken from the initial temperature 4.

Table 4 Particle Heating Time Scale

Particle	Time (s)
1	3.26654×10^{-6}
2	2.79812×10^{-4}
3	5.58656×10^{-3}
4	1.9448×10^{-2}
5	3.68134×10^{-2}

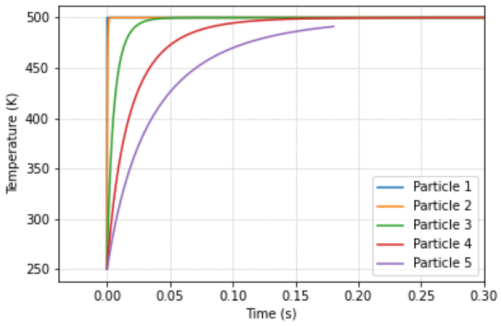

Fig. 7 Evolution of particle Temp vs time for inert injection

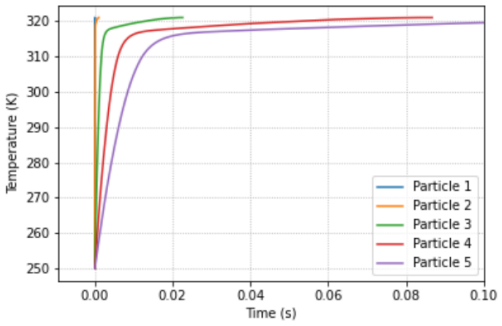

Fig. 8 Evolution of particle Temp vs time for evaporation injection

Observations indicate that particle 1 reaches its maximum temperature quicker compared to the others, in both cases of inert injection and evaporation model. Furthermore, the time required to reach maximum temperature gradually increases for particles 2, 3, 4, and 5, in line with their ascending sizes. In Accordance to equation8, the time taken to reach maximum temperature is directly proportional to the initial diameter of the particles. Fluent simulations provide values of $T_{n,b}$ and $T_{eva\,p}$ as 351 K and 271 K, respectively.

In this scenario of injection with evaporation model, the recorded maximum temperature of 320.95 K exceeds $T_{eva\,p}$, yet remains below T_b. Consequently, this scenario aligns with law 2, as outlined in section II.B, indicating evaporation occurs via an infinite conduction model (see Fig.8).

D. Equilibrium temperature for an evaporating droplet

It's important to recognize that when a droplet evaporates, it achieves a temperature denoted as T_{eq}, which might differ from the boiling temperature of the liquid under the prevailing pressure. This temperature can be approximated by assuming a Lewis number of 1, resulting in equal Spalding numbers for both thermal and mass transfer.

$$BT = \frac{C_{pg} \cdot (T^{\infty} - T_l^s)}{L_v} = BM = \frac{Y^s - Y^{\infty}}{1 - Y^s} \tag{9}$$

The mass fraction Y^s represents the amount of vapor at the surface of the droplet, while Y^{∞} denotes the mass fraction of vapor far from the droplet, which is assumed to be zero in our scenario. The value of Y^s can be determined from the molar fraction x_s and the molar masses M_{vap} and M_{air}.

$$Y_s = \frac{x_s M_{\text{vap}}}{x_s M_{\text{vap}} + (1 - x_s) M_{\text{air}}} \tag{10}$$

The molar fraction at the droplet surface x^s can be obtained by considering that the partial pressure of vapor is equal to the saturation pressure of the liquid. The saturation pressure is determined by the Clausius-Clapeyron law, which is a function of the normal boiling temperature T_{nb} and the (unknown) equilibrium temperature T_{eq}:

$$x_s \cdot p_g = p_{\text{sat}} \tag{11}$$

$$K_d = -\frac{d}{dt} d_p^2 = 4 \lambda_g \rho_l c_p N_u \cdot \ln(1 + B_T) \tag{12}$$

The equilibrium temperature T_{eq} determined from Fig.9 is 304 K. In Fluent, the temperature reached is slightly higher at 310 K, as observed in Fig.8. Comparing these temperatures reveals a small deviation.

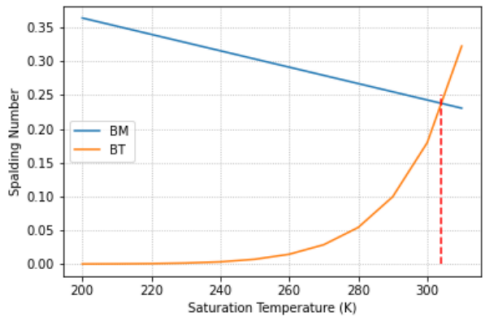

Fig. 9 Spalding transfer number vs temperature

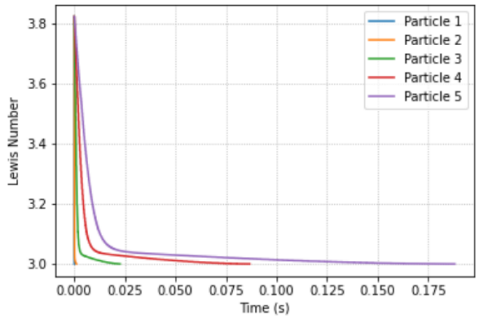

Fig. 10 Particle Lewis number vs temperature

The Lewis number is defined as the ratio of the thermal diffusivity to the mass diffusivity and it predicts the behavior of combustion and heat transfer in the systems. The Lewis number is important because it helps to determine the relative magnitudes of heat transfer, mass transfer, and reaction rate, which are critical in the modeling of combustion processes. Fig.10 shows the evolution of Lewis-number in time when the binary diffusivity of the droplet particle is set to constant.

While the Lewis number is imposed to be 1, there is no variation in time. Figure.11 Evolution of particle temperature vs time, in this case. The Lewis number being 1 indicates a situation where heat and mass transfer occur at the same rate because of identical thermal and mass diffusivity. It results in temperature changes and evaporation/condensation happening concurrently. Moreover the properties for the gas mixture strongly change close to the droplet. While unit-Le simplifies problem analysis, it may not accurately represent real-world behavior, given that heat and mass diffusivity typically differ.

The equilibrium temperature is influenced by the vapor mass diffusivity coefficient as it impacts the rate of vapor transfer from a hot surface to a cooler one. A higher vapor mass diffusivity coefficient facilitates rapid and efficient vapor transport, leading to a smaller temperature difference between the hot and cool surfaces. Conversely, a lower vapor mass diffusivity coefficient leads to slower transport and a larger temperature difference between the hot and cool surfaces.

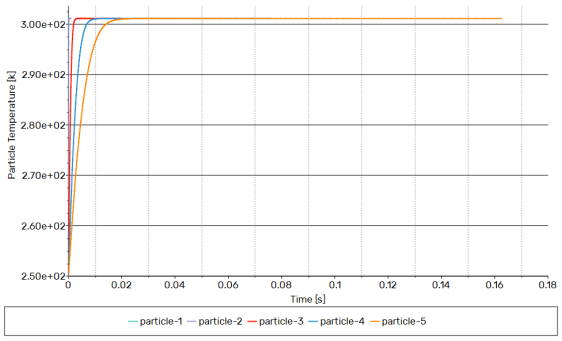

Fig. 11 Particle temp vs time (Unit Lewis number)

E. Evaporation Rate

The expression of the evaporation rate as per the d^2 law is given below:

$$K_d = -\frac{d}{dt}d_p^2 = 4\lambda_g \rho_l c_p N_u \cdot \ln(1 + B_T) \tag{13}$$

For the varied values of B_T achieved from the T_{eq}, the K_d are calculated using the given Equ.13. The values are as tabulated in Table5.

Table 5 Evaporation rate using the d^2 law.

$T_(eq)$	B_T	P_sat	x_s	Y_s	B_M	K_d
200	0.36421	3.86007	0.00004	0.00006	0.00006	1.38E-07
210	0.35207	11.90557	0.00012	0.00019	0.00019	1.34E-07
220	0.33993	33.14644	0.00033	0.00052	0.00052	1.30E-07
230	0.32779	84.42191	0.00083	0.00133	0.00133	1.26E-07
240	0.31565	198.90176	0.00196	0.00313	0.00314	1.22E-07
250	0.30351	437.56986	0.00432	0.00687	0.00692	1.17E-07
260	0.29137	905.97674	0.00894	0.01419	0.01439	1.13E-07
270	0.27923	1777.35479	0.01754	0.02769	0.02848	1.09E-07
280	0.26709	3322.97545	0.03280	0.05131	0.05408	1.05E-07
290	0.25495	5950.29571	0.05872	0.09050	0.09951	1.01E-07
300	0.24281	10249.02467	0.10115	0.15218	0.17949	9.63E-08
310	0.23067	17044.78123	0.16822	0.24390	0.32257	9.19E-08

When assuming $\mathrm{Nu}^* = 2$, the parameter K_d remains unaffected by changes in droplet diameter. However, this assumption holds true only when the Reynolds number (Rep_p) is significantly less than 1.

Convection has significant effects on vaporization, as it strongly effects the mass and energy transfer. But all the droplet vaporization models uses the spherical symmetry hypothesis, which is not compatible with the convection effects. Using the "film theory", corrections factors are added to the d^2 law with variable properties for gas mixture, to take into account convection effects, while considering the spherical symmetry. The film theory considers the presence of boundary layers, whose thickness for mass and energy transfers are defined respectively by:

$$\delta M = \frac{D_d}{\mathrm{Sh}_0 - 2} \tag{14}$$

$$\delta T = \frac{D_d}{\mathrm{Nu}_0 - 2} \tag{15}$$

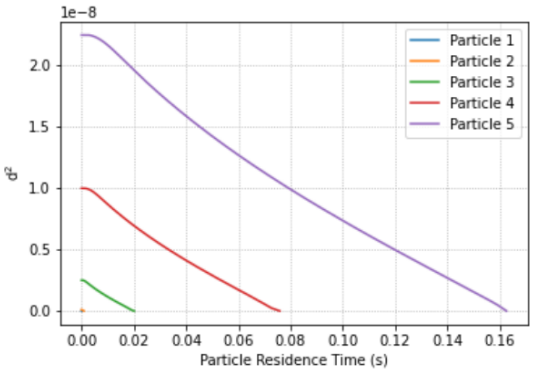

Fig. 12 d_p^2 vs time for particles with different diameter

The Sherwood (Sh_0) and Nusselt (Nu_0) Numbers without "Stefan Flow" are the radial flow at the droplet surface due to vaporization. (Sh_0) and (Nu_0 are often calculated from Reynolds, Schmidt and Prandlt in Ranz-Marshall correlations to address this issue by adjusting the droplet Nusselt number.

$$Sh_0 = 2 + 0.6 \cdot \mathrm{Re}^{1/2} \cdot \mathrm{Sc}^{1/3} \tag{16}$$

$$Nu_0 = 2 + 0.6 \cdot \mathrm{Re}_p^{1/2} \cdot \mathrm{Pr}^{1/3} \tag{17}$$

The Stefan Flow modifies the thickness of the boundary layers and modified Nusselt numbers is:

$$\mathrm{Nu}^* = 2 + \frac{\mathrm{Nu}_0 - 2}{F(B_T)} \tag{18}$$

where

$$F(BT) = \frac{\ln(1+BT)}{BT} \cdot (1+BT)^{0.7} \tag{19}$$

The linear behaviour in the Fig.12 can be observed to be post the 50% of the particle residence time. The reason could be the gas ambient conditions and droplet temperature and compositions are constant. This possibly means that the droplet is in a controlled environment with uniform temperature and the rate of heat and mass transfer to and from the droplet is constant and well-defined after given time.

III. Dispersed, Reactive Spray Flow Combustion

A. Introduction

The focus of this practical session is to perform a CFD simulation of reactive spray flow in the vicinity downstream of a V-shaped flame holder bluff body within a channel. The simulation aims to analyze the turbulent flow and recirculation zones that arise due to the flame holder's trailing edges. The interaction between the kerosene-air mixture and the combustion process will be modeled using steady-state RANS with an eddy-dissipation model for combustion, complemented by discrete phase models to address spray transport and evaporation.

B. Results

The contour plots showing the turbulent reaction rate reveals a band-like region downstream of the air stream with a reaction rate higher than the surrounding areas14. This is typical in the wake of bluff bodies like flame holders. The recirculation zone can trap reactants and products, creating a local environment where the reaction can continue. The band-like region of the high turbulent rate of reaction corresponds to the location of the shedding shear layer. The banded area is consistent with the area of high static temperature shown in Fig. 13. The highest reaction rate locates close to where the highest temperature gradient locates, and the high temperature region is found downstream the

flame within the region the reaction is finished due to the time required for the heat to be released from the exothermic reactions.

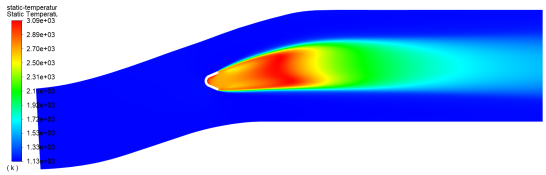

Fig. 13 Static Temperature

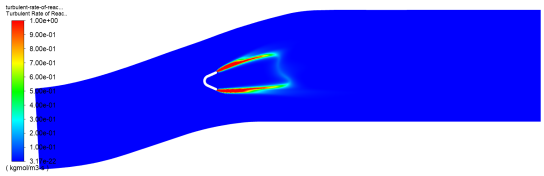

Fig. 14 Turbulent Rate of Reaction

The mass fraction contours of O_2 and $C_{12}H_{23}$ are plotted to investigate the adequacy of combustion 15 16. The region with high concentration of $C_{12}H_{23}$ is mainly located in the wake of the flame holder, which means there is still $C_{12}H_{23}$ left after the reaction. In the wake of flame holder the concentration of O_2 is almost reduced to zero which is consistent. The local equivalence ratio is shown in Fig. 17, which is defined by Eq. 20, assuming $s \approx 14.7$ for kerosene. The range of the color bar is from 0 to 2. It is obvious that only around the flame front the equivalence ratio is around 1.

$$\phi = s\frac{Y_F}{Y_{O_2}} \tag{20}$$

1. Fuel Mass Flow Rate

Assuming the fuel is injected at the burnt gas temperature, Eq. 21 is applied.

$$\dot{m} \cdot c_p \cdot (T_{t,out} - T_{t,0}) = \dot{m}_f \cdot H_f \tag{21}$$

The inlet conditions are listed $\dot{m} = 4.75$ kg/s, $T_{t,0} = 1184$ K and the increase in temperature is $\Delta T_t = 300$ K. The fuel lower heating value is $H_f = 43200$ kJ/kg and the specific heat capacity of air is $c_p = \gamma \cdot r/(\gamma - 1)$ assumed to be constant with $\gamma = 1.35$ at the inlet temperature and $r = 287.04$ J/kg/K.

Therefore, the total fuel mass flow rate required is calculated to be $\dot{m}_{f,0} = 1.826 \times 10^{-2}$ kg/s.

2. Adequacy of Combustion

An integral of the mass fraction of $C_{12}H_{23}$ at the outlet is performed to obtain the mass flow rate of unburnt fuel, which is $\dot{m}_{f,1} = 1.883 \times 10^{-5}$ kg/s. The proportion of unburnt fuel to the total injected fuel flow was only 0.103%.

3. Modification of the Heat Equation

A mass-weighed average of the total temperature at the outlet is calculated to analyze the temperature increase predicted by the simulation. The result turned out to be $T_{t,out} = 1312.0$ K, which indicates an increase of $\Delta T_{t,real} = 128.0$ K. This is a considerable decrease than the expected temperature increase. From the integral of the mass fraction of $C_{12}H_{23}$ at the outlet we found out the fraction of unbrunt fuel is negligible, which can be approximated as complete combustion.

The simplified heat equation used in this study is based on a premixed flame. Whereas in practice, the fuel is injected from liquid form into the gas stream for diffusion combustion. The presence of liquid droplets in the form of fuel spray can lead to additional heat transfer mechanisms such as latent heat of vaporization which are not considered in the simplified energy balance equation. A correction term for the heat of vaporization Q_{vap} is needed to be added to the left side of the equation, leading to a modified equation Eq. 22.

$$\dot{m} \cdot c_p \cdot (T_{t,out} - T_{t,0}) + Q_{vap} = \dot{m}_f \cdot H_f \tag{22}$$

References

[1] CT Crowe. *Vapor-droplet flow equations*. Tech. rep. California Univ., Livermore (USA). Lawrence Livermore Lab., 1975.

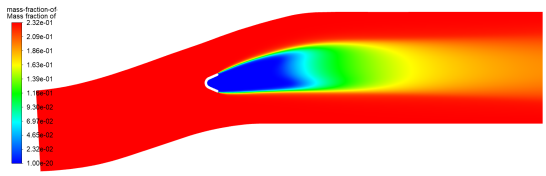

Fig. 15 Mass fraction of O_2

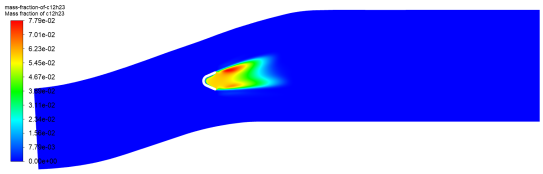

Fig. 16 Mass fraction of $C_{12}H_{23}$

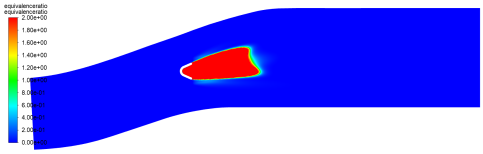

Fig. 17 Equivalence Ratio